1006 J. Phys. Chem. 1990, 94, 1006-1010

Evidence for an Ag_4O_3 Phase of Silver Oxide

A. N. Mansour[†]

Research and Technology Department, Naval Surface Warfare Center, 10901 New Hampshire Avenue, Silver Spring, Maryland 20903-5000 *(Received: March 6, 1989; In Final Form: June 20, 1989)*

The structure of chemically and electrochemically prepared AgO materials was investigated by extended X-ray absorption fine structure (EXAFS) spectroscopy. It was found that chemically prepared (CP) AgO is composed of Ag^+ and Ag^{3+} ions coordinated with two oxygens at 2.13 Å and four oxygens at 1.99 Å, respectively. For electrochemically prepared (EP) AgO, the Ag^+ ions are also coordinated with two oxygens at a distance of 2.13 Å. However, the coordination number for the Ag^{3+} ions varies from 2.8 to 3.5 oxygens without any significant change in the coordination distance of 1.99 Å. That is, EP AgO is really $AgO_{1-\delta}$, where δ is the degree of oxygen deficiency near the Ag^{3+} ions. The magnitude of δ can be as large as 0.29 ± 0.05 and is a strong function of preparation procedures. The EXAFS results reveal that a phase of silver oxide, Ag_4O_3, is formed electrochemically. The EXAFS results also suggest that the electrochemical oxidation of Ag or Ag_2O to AgO proceeds via the formation of Ag_4O_3 as an intermediate step.

Introduction

Silver oxide/zinc alkaline batteries are used as primary power sources in many commercial and military applications due to their high energy and power densities.[1] Electrochemically prepared (EP) AgO materials are used for high-rate applications and are prepared by the constant-current anodization of either sintered Ag or a paste of Ag_2O.[2] Chemically prepared (CP) AgO materials, on the other hand, are used for low-rate applications and are prepared by oxidizing alkaline $AgNO_3$ solutions with ozone[3] or persulfate.[4] The fact that EP AgO materials are thermally less stable than CP AgO materials has been a major concern to battery manufacturers for many years because the high decomposition rate of EP AgO cathodes during battery storage is responsible for performance degradation problems. AgO decomposes to form Ag_2O, which has a much higher ohmic resistance than AgO and causes a voltage regulation problem. The liberated O_2 gas may react with the Zn anode, forming a film of ZnO that causes voltage delay. The large variations observed in thermal stability of EP AgO materials under dry conditions have been found to depend on preparation procedures.[5]

Electrochemically induced variations in the structure of EP AgO from that of CP AgO material could play an important role in characterizing the factors contributing to the enhanced decomposition rate. An improved knowledge of the structure of EP AgO material could prove invaluable to the solution of the thermal instability problem. The electrochemical preparation procedures could then be tailored to the preparation of highly stable materials.

The crystal structure of AgO has been studied both by X-ray[6,7] and neutron[8] diffraction techniques. Neutron diffraction of a very slightly oxygen-deficient AgO ($AgO_{1-\delta}$ with $\delta = 0.025$) prepared by an ozonization process more precisely determines the position of the oxygen atoms than does X-ray diffraction. This is so because silver and oxygen have nearly equal nuclear scattering amplitudes, while the X-ray scattering cross section of silver overwhelms that of oxygen. Neutron diffraction indicates that the correct space group for AgO is $C_{2h}{}^5(P2_1/c)$ rather than $C_{2h}{}^6$ as determined by the X-ray diffraction work. The neutron diffraction data were interpreted in terms of a monoclinic lattice with four molecules of AgO in a unit cell with silver equally distributed between the 1+ and 3+ oxidation states. On the basis of this structure, AgO is usually described by the $Ag_2{}^IO-Ag_2{}^{III}O_3$ formula to emphasize the dual valency of Ag in AgO responsible for its diamagnetic behavior. In the neutron diffraction study, no evidence was found to substantiate the existence of a previously reported ZnS structure[9,10] in which silver ions are coordinated with four oxygen ions at 2.08 Å.

Extended X-ray absorption fine structure (EXAFS) has been widely used for determining the local structure in a large class of materials.[11-13] The structure of both crystalline and amorphous materials can readily be investigated. EXAFS explores the modulations in the X-ray absorption spectrum that extend from approximately 40 eV above the X-ray absorption edge up to about 1000 eV or more. Analysis of these modulations yeilds quantitative information regarding the structure of the first few coordination spheres adjacent to the central absorbing atom. In particular, EXAFS determines the coordination number (N), coordination distance (R), disorder (defined as the root mean square deviations in the coordination distance, σ), and the identity of neighboring atoms. Because of its sensitivity to short-range structure, EXAFS is uniquely suited to the investigation of small differences between the local structure of Ag in EP AgO and that in CP AgO.

The purpose of this paper is to examine the structure of CP AgO and to determine the structure of the first coordination sphere in EP AgO as a function of preparation procedures. In addition to EXAFS analysis, all samples were analyzed by X-ray diffraction.

Experimental Procedure

The EP AgO samples were produced by constant current anodization of both unpressed and pressed sintered silver metal plates.[2] Scanning electron microscopy (SEM) micrographs show that unpressed plates are more porous and have a higher surface area than pressed plates. Several plates of each type were charged at room temperature in 31 or 40 wt % KOH and at the apparent surface current densities indicated in Table I. A typical constant current anodization produced a voltage vs time curve with three voltage plateaus. The principal reaction at the lower potential plateau is the oxidation of silver metal to monovalent silver oxide

---

[†] Correspondence should be sent to the following address: Naval Surface Warfare Center, 10901 New Hampshire Ave., Code R34, Bldg. 30, Rm 213, Silver Spring, MD 20903-5000.

(1) Howard, P. L. In *Zinc-Silver Oxide Batteries*; Fleischer, A., Lander, J. J., Eds.; Wiley: New York, 1971; pp 371-373.

(2) Falk, S. U.; Fleischer, A. In *Zinc-Silver Oxide Batteries*; Fleischer, A., Lander, J. J., Eds.; Wiley: New York, 1971; pp 199-207.

(3) McKie, A. S.; Clark, D. In *Batteries*; Collins, D. H., Ed.; MacMillan: New York, 1963; pp 285-295.

(4) Hammer, R.; Kleinberg, J. In *Inorganic Syntheses*; Bailar, J. C., Jr., Ed.; McGraw-Hill: New York, 1953; pp 12-14.

(5) Dallek, S.; West, W. A.; Larrick, B. F. *J. Electrochem. Soc.* **1986**, *133*, 2451.

(6) Graff, W. S.; Stadelmaier, H. H. *J. Electrochem. Soc.* **1958**, *105*, 446.

(7) McMillan, J. A. *Acta Crystallogr.* **1954**, *7*, 640.

(8) Scatturin, V.; Belon, P.; Salkind, A. J. *J. Electrochem. Soc.* **1961**, *108*, 819.

(9) Stehlik, B.; Weidenthaler, P. *Collect. Czech. Chem. Commun.* **1957**, *24*, 1416.

(10) Stehlik, B.; Weidenthaler, P. *Chem. Listy* **1958**, *52*, 402.

(11) Stern, E. A. In *X-Ray Absorption, Principles, Applications, Techniques of EXAFS, SEXAFS And XANES*; Koningsberger, D. C., Prins, R., Eds.; Wiley: New York, 1988; pp 3-51.

(12) Sayers, D. E.; Stern, E. A.; Lytle, F. W. *Phys. Rev. Lett.* **1971**, *27*, 1204.

(13) Lee, P. A.; Citrin, P. H.; Eisenberger, P.; Kincaid, B. M. *Rev. Mod. Phys.* **1981**, *53*, 769.

TABLE I: Summary of Charging Conditions for the Electrochemically Prepared AgO Samples

sample no.[a]	KOH, wt %	current, mA/cm^2	duration of C or D,[b] min	time to AgO, min	time to O_2 evolution, min	duration of O_2 evolution, min
EP-2 (UNPR)	31	2.59	416 (C)	55	416	0
EP-3 (UNPR)	31	2.86	600 (C)	49	369	231
		3.52	60 (D)			
		2.43	300 (C)			
EP-4 (UNPR)	31	2.73	482 (C)	76	406	
		3.52	60 (D)			
		2.43	300 (C)			
EP-5 (PR)	40	3.00	580 (C)	39	272	308
EP-6 (PR)	40	3.00	300 (C)	28	296	4
EP-7 (PR)	40	0.74	1400 (C)	252	1371	29

[a] UNPR and PR refer to unpressed and pressed sintered silver plates, respectively. [b] C or D refer to charge or discharge cycles, respectively.

(Ag_2O). This plateau continues until the surface is completely covered with Ag_2O. Then the voltage increases sharply, going through a sharp maximum before leveling off at the higher potential of the second plateau. At this potential, it is believed both oxidation of Ag_2O to AgO and of Ag to Ag_2O occur. Finally, oxygen evolution near the electrode surface is observed at the third and highest potential plateau. During prolonged oxygen evolution, some oxygen can still be added to the electrode[14,15] and is believed to improve the crystallinity of AgO.[16] The EP samples (3 and 4) were charged, discharged, and then charged again as indicated in Table I. All of the charged (finished) electrodes were given a final rinse in deionized, distilled water to remove the KOH electrolyte. The CP AgO sample investigated in this study was produced by oxidizing $AgNO_3$ with $Na_2S_2O_8$ in an alkaline solution. A sample of CP Ag_2O was used as a standard for subsequent EXAFS data analysis.

All samples were characterized by X-ray diffraction. The radiation was produced by a copper anode with a nickel foil filter. For the X-ray absorption measurements, the fine powdered material was spread on KAPTON tape (trademark of 3M Corp., St. Paul, MN) so only one layer of the material adhered to the tape. Several layers were then stacked to make an optimal thickness for the X-ray absorption measurements.[17] The X-ray absorption measurements were performed at the National Synchrotron Light Source (NSLS) on beam line X11-A using a double-crystal monochromator with Si(400) crystals and operating with typical electron currents of 40–80 mA at 2.52 GeV.[18] Spectra of the silver K edge (25.514 keV) were measured in the transmission mode at temperatures of 298 and 135 K. Each spectrum required a collection time of approximately 20 min.

Data Analysis

The normalized EXAFS data, $\chi(k)$, are extracted from the experimentally measured X-ray absorption spectra according to

$$\chi(k) = (\mu(k) - \mu_0(k))/\Delta\mu_0$$

where μ is the total X-ray absorption coefficient measured above an absorption edge, μ_0 is the slowly varying component of μ due to absorption by the central absorbing atom, the step increase in X-ray absorption edge $\Delta\mu_0$ is used to normalize the EXAFS data to a per metal atom basis, and k is the photoelectron wavenumber. For polycrystalline materials and in the dipole approximation, the EXAFS spectrum is related to the structural properties of the sample by the relation

$$\chi(k) = \sum_i (N_i/kR_i^2)A_i(k) \exp(-2R_i/\lambda) \exp(-2\sigma_i^2k^2) \times \sin(2kR_i + 2\phi_i(k))$$

where the index i denotes a specific type of atom located at an average distance R_i from the central absorbing atom and N_i is the number of atoms of the ith type at distance R_i. The term σ_i is the disorder or root mean square deviation about the average distance R_i and includes both a dynamic term arising from the thermal motion of the atoms and a static term describing structural disorder. The other terms λ, $A_i(k)$, and $\phi_i(k)$ are the electron mean free path, the magnitude of the backscattering amplitude for the ith type of atoms, and the phase shift due to alteration of the wave function of the ejected photoelectron by the potential of the absorbing and scattering atoms, respectively. Methods of analysis of experimental spectra are discussed in detail elsewhere.[19,20] Briefly, the zero of energy was taken to be at the half-height of the X-ray absorption edge. The nonoscillatory portion of the absorption spectrum was removed by fitting the data above the edge with a segmented (five segments) smooth cubic spline function, leaving the oscillatory EXAFS function $\chi(k)$. This was followed by a Fourier transformation of $k^3\chi(k)$ over a range of k determined by the quality of the experimental data. Finally, the dominant frequencies in the Fourier transform corresponding to the first few Ag–O shells were filtered from the transformation. The filtered data were then Fourier transformed back to k space where the atomic structure was determined by a least-squares fit to a parametrized form of the EXAFS formula.

TABLE II: Summary of XRD Analysis of Electrochemically Prepared AgO Cathodes

	cathode composition, mol %				peak broadening	
sample no.	AgO	Ag_2CO_3	Ag_2O	Ag	fwhm$_1$[a]	fwhm$_2$[b]
CP–AgO	97.8	2.2	0.0	0.0	0.18	0.20
EP-2	93.8	1.6	2.1	2.5	0.25	0.26
EP-3	97.5	1.4	0.5	0.6	0.26	0.26
EP-4	94.9	2.4	1.3	1.4	0.25	0.26
EP-5	94.1	0.0	1.0	5.0	0.27	0.25
EP-6	93.2	0.0	1.7	5.1	0.32	0.32
EP-7	97.8	0.0	0.0	2.2	0.27	0.25

[a] fwhm$_1$: the full width at half-maximum of the most intense Bragg line for the AgO$(11\bar{1})$ plane, accurate to ±0.02. fwhm$_2$: the full width at half-maximum of the second most intense Bragg line for the AgO(111) plane, accurate to ±0.02.

Results

The X-ray diffraction pattern obtained for the CP AgO sample agreed with published data for CP AgO materials.[6,8] The Bragg diffraction lines for EP AgO coincided with those characteristic of CP AgO but with larger full widths at half-maximum (Table II). Thus, all samples of EP AgO consisted mainly of a single phase of AgO with the same lattice parameters as CP AgO. In addition, the X-ray data include lines consistent with at least one of the phases, Ag_2CO_3, Ag_2O, or Ag being present as a minor impurity in all of the AgO materials (see Table II). As a result of broadening, the EP AgO peak at $2\Theta = 32.07°$ was not resolved from the peak at $2\Theta = 32.34°$ and was usually observed only as

---

(14) Dirkse, T. P. *J. Electrochem. Soc.* **1959**, *106*, 920.
(15) Dirkse, T. P. *J. Electrochem. Soc.* **1960**, *107*, 859.
(16) Wales, C. P.; Burbank, J. *J. Electrochem. Soc.* **1959**, *106*, 885.
(17) Stern, E. A.; Kim, K. *Phys. Rev. B* **1981**, *23*, 3781.
(18) Sayers, D. E.; Heald, S. M.; Pick, M. A.; Budnick, J. I.; Stern, E. A.; Wong, J. *Nucl. Instrum. Methods* **1983**, *208*, 631.
(19) Sayers, D. E.; Bunker, B. A. In *X-Ray Absorption, Principles, Applications, Techniques of EXAFS, SEXAFS And XANES*; Koningsberger, D. C., Prins, R., Eds.; Wiley: New York, 1988; pp 211–253.
(20) Cook, J. W., Jr.; Sayers, D. E. *J. Appl. Phys.* **1981**, *52*, 5024.

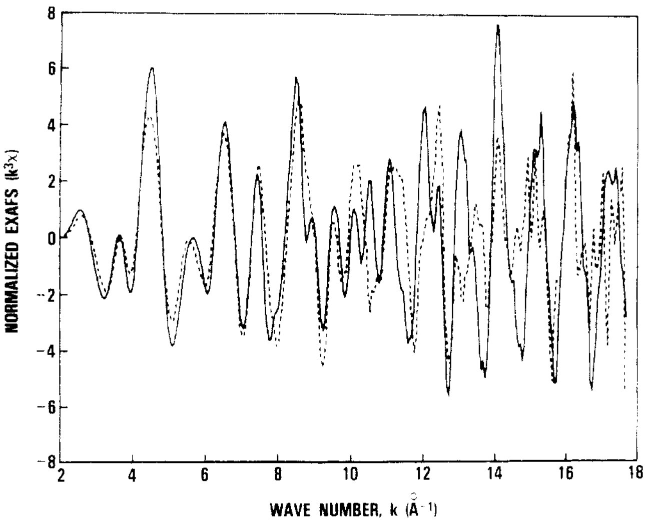

Figure 1. Comparison of normalized k^3-weighted EXAFS data versus the photoelectron wavenumber for CP AgO (solid) and EP AgO (sample EP-5) (dash) taken in the transmission mode at 135 K.

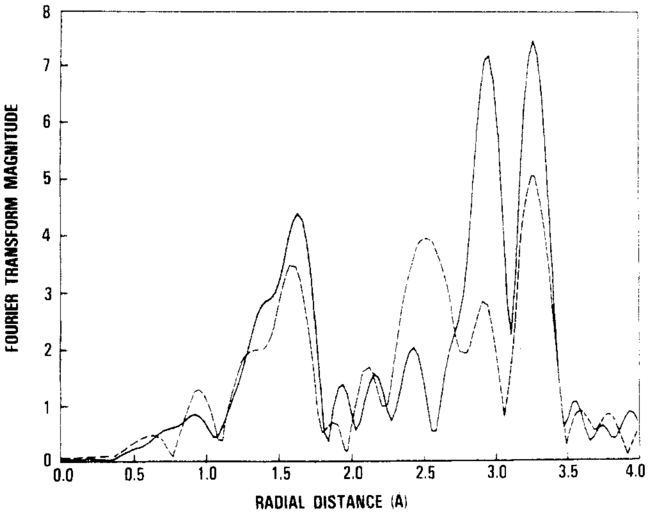

Figure 2. Fourier transform magnitudes of k^3-weighted EXAFS data taken at 135 K for CP AgO (solid) and EP AgO (sample EP-5) (dash) over the k range of 2.1–17.6 Å^{-1}.

a shoulder on the main peak ($2\Theta = 32.34°$). These two peaks were well resolved in the X-ray diffraction pattern of CP AgO. The degree of broadening was also found to vary as a result of differing preparation procedures. Variations in the full width at half-maximum of the Bragg diffraction peaks (Table II) could be due to either variations in details of the local structure or to particle size effects. Scanning electron microscopy micrographs show that the average size of the AgO crystallites is too large (>1 μm) to account for the broadening of the peaks. Hence, the broadening must be due to variations in the details of the structure.

Figure 1 shows a comparison of the normalized k^3-weighted EXAFS data, $k^3\chi(k)$ taken at 135 K for CP AgO and EP AgO. The $k^3\chi(k)$ data is plotted versus the photoelectron wavenumber k after subtraction of the smooth background above the silver K edge from the X-ray absorption data. The data indicates that the frequencies of the normalized $\chi(k)$ for the two samples are qualitatively the same. However, significant differences are clearly visible in the amplitude of the EXAFS signal for CP and EP AgO. For low k values (<7 Å^{-1}) in which the EXAFS signal is dominated by scattering from oxygen nearest-neighbors, the EP AgO amplitude of the EXAFS is significantly smaller than that of CP AgO. These differences in the amplitude of the EXAFS signal arise from changes in the coordination number as will be shown later.

Figure 2 shows Fourier transforms of the $k^3\chi(k)$ data of Figure 1 over the k range of 2.1–17.6 Å^{-1}. The coordination number (N), type of atom (Z), and the distance (R) for the first few coordination spheres around the Ag^{1+} and Ag^{3+} ions of CP AgO as determined from neutron diffraction data[8] are listed in Table III. In this table, the oxygen atoms are labeled O(1) and O(2) to differentiate between oxygen atoms shared between immediately adjacent Ag^+ and Ag^{3+} and those only coordinating the Ag^{3+}, respectively. The Ag^{3+} ions are coordinated in a square-planar arrangement with four oxygen atoms at an average distance of 2.034 Å. Two of these oxygen atoms (i.e., the O(1)'s) are also coordinating the Ag^+ ions at a distance of 2.179 Å. Therefore, in the Fourier transform, the peak that encompasses the r space of 1.07–1.87 Å is due to Ag–O interactions at 2.034 and 2.179 Å. The group of peaks extending over r space from 1.87 to 2.57 Å arise from the Ag–O interactions at 2.645, 2.771, and 2.894 Å. The two peaks between 2.57 and 3.50 Å are the result of Ag–Ag interactions at 3.252, 3.358, 3.404, and 3.478 Å. The shift in the peak positions from their real crystallographic distances to lower values is an artifact of the EXAFS analysis procedure. Inasmuch as the positions of the peaks in the Fourier transform of EP AgO are the same as those of CP AgO, both types of AgO share the same crystal lattice, in agreement with XRD analyses. However, the amplitude of the EP AgO peaks are significantly lower than those for CP AgO. The only case where an EP peak is larger than the CP peak is the one at approximately 2.5 Å, which is due to uncharged (e.g., metallic) silver. The presence of metallic silver is also indicated by X-ray diffraction analysis (Table II).

TABLE III: Summary of Coordination Number (*N*), Distance (*R*), and Type of Atoms (*Z*) for the First Few Coordination Spheres (*i*) in AgO and Ag_2O

	Ag^+			Ag^{3+}		
i	*N*	*Z*	*R*, Å	*N*	*Z*	*R*, Å
			AgO[a]			
1	2	O(1)	2.179	2	O(1)	2.013
2	2	O(2)	2.645	2	O(2)	2.054
3	2	O(1)	2.894	2	O(1)	2.771
4	4	Ag^+	3.252	4	Ag^{3+}	3.252
5	2	Ag^{3+}	3.358	2	Ag^+	3.358
6	4	Ag^{3+}	3.404	4	Ag^+	3.404
7	2	Ag^+	3.478	2	Ag^{3+}	3.478
			Ag_2O[b]			
1	2	O	2.044			
2	12	Ag^+	3.338			

[a] Determined using structural data in ref 8. [b] Determined using structural data in ref 21.

Quantitative analysis methods are presented here for the structural information contained in the first peak of the Fourier transform (i.e., $\Delta r = 0.8–1.9$ Å), which was isolated and transformed back into k space to allow quantitative analysis of k-space amplitudes and phases. The back-transformed data was then fitted with two shells of Ag–O interactions. One shell corresponded to the local structure around the Ag^+ ions and the other to the structure around the Ag^{3+} ions. Because of the equivalency of the two oxygen atoms in the first coordination sphere of Ag_2O (Table III),[21] this compound was used to extract the backscattering amplitudes and phase values necessary to model the Ag–O interactions with the least-squares fitting program. In determining coordination numbers and bond lengths, it is necessary to assume amplitude and phase transferability between the standard (i.e., Ag_2O) and compounds being analyzed. Amplitude transferability is a well-established principle which, although not always valid, holds for chemically and structurally similar systems.[22] Phase transferability is more generally applicable than amplitude transferability and is valid for a wide range of systems that are significantly different chemically.[23] Ag_2O is a useful standard for AgO, both because of the chemical similarity and because the

---

(21) Wyckoff, R. W. G. *Crystal Structures*, 2nd ed.; Interscience: New York, 1963; Vol. 1.

(22) Eisenberger, P.; Lengler, B. *Phys. Rev. B* **1980**, *22*, 3551.

(23) Citrin, P. H.; Eisenberger, P.; Kincaid, B. M. *Phys. Rev. Lett.* **1976**, *36*, 1346.

TABLE IV: Results of Numerical Fits to the Filtered EXAFS Data for the Ag^+ and Ag^{3+} Ions in CP and EP AgO[a]

	Ag^+		Ag^{3+}		
sample no.	N_1	R_1, Å	N_2	R_2, Å	δ
CP-1	2.00	2.13	3.93	1.99	0.02
EP-2	1.98	2.13	3.38	1.99	0.16
EP-3	2.09	2.13	3.50	1.99	0.13
EP-4	1.88	2.13	3.35	1.99	0.16
EP-5	1.95	2.12	2.83	1.99	0.29
EP-6	2.08	2.11	3.02	1.99	0.25
EP-7	1.92	2.13	3.27	1.99	0.18

[a] N_i and R_i are the average of the values obtained from fitting the 135 and 298 K data. Uncertainties are as follows: N_i, ±5%; R_i, ±0.02; δ, ±0.05.

first two shells in the Ag_2O Fourier transform are completely resolvable and its higher shells are relatively weak. These characteristics minimize errors due to interference of peaks in the Fourier transform.

In the fitting procedure, four parameters per shell usually need to be varied: coordination number (N), coordination distance (R), relative disorder squared ($\Delta\sigma^2$), and an inner potential energy shift (E_0) which is used in the definition of k [$k = ((2m/\hbar^2)(E - E_0))^{1/2}$, where E is the kinetic energy of the photoelectron]. Thus, for a two-shell fit, we have eight parameters to fit, but the restricted k range of the reliable k data precludes meaningful fits to so many parameters. However, we have independent knowledge of some parameters ($\Delta\sigma^2$) and expect others (E_0) to be well-behaved, lying within a relatively narrow range. The characteristics of the real structure that are most likely to vary are N_1, N_2, R_1, and R_2. Thus, we choose to make the problem tractable by fixing $\Delta\sigma^2$ and E_0 at reasonable values (which we justify here) and fit only the N and R. The disorder for the Ag–O interactions in AgO, relative to that in Ag_2O at 298 K, was determined from CP AgO data with structural information known from neutron diffraction.[8] The values for the relative disorders were $\Delta\sigma_1^2 = \Delta\sigma_2^2 = -0.0020$ Å^2 for the 135 K data and −0.0017 Å^2 for the 298 K data. The validity of applying relative disorder values from CP AgO data to EP AgO data was confirmed by checking the sensitivity of N_1, N_2, R_1, and R_2 to variations in the values of $\Delta\sigma_1^2$ and $\Delta\sigma_2^2$ over a range of ±50%. Over this range of disorder, R_1 and R_2 remained the same while N_1 and N_2 varied less than 5%. All fits were done in the k range of 3–11 Å^{-1} with k^3-weighted inverse data. Each fit was performed at successive values of the inner potential (E_0) until an optimum fit was obtained. An optimum fit (defined here as that converging fit with the smallest value for the sum of the square of residuals between the experimental and calculated data) was obtained for $E_0 = 0.0$ for both shells (i.e., no inner potential shift was needed). Results of numerical fits to the back-transformed data are listed in Table IV. Typical fits for CP and EP AgO are shown in Figures 3 and 4, respectively.

Discussion

We conclude for CP AgO the Ag^+ and Ag^{3+} ions are coordinated with two oxygens at 2.13 Å and four oxygens at 1.99 Å, respectively. This is in agreement with the results of neutron diffraction[8] except for a slightly smaller (approximately 0.04 ± 0.02 Å) coordination distance. The results for EP AgO also show the Ag^+ ions to be coordinated with two oxygens at a distance of 2.13 Å. However, the coordination number for Ag^{3+} varies from 2.8 to 3.5 oxygens without any significant change in the coordination distance. We conclude that EP AgO is highly oxygen-deficient relative to CP AgO and that all the oxygen-vacant sites are near Ag^{3+} ions. That is, EP AgO is really $AgO_{1-\delta}$ where δ, the degree of oxygen deficiency, is determined by

$$\delta = [4 - N_2]/4$$

and is a function of only the coordination number N_2 of the Ag^{3+} ions. The results displayed in Table IV demonstrate that δ can be as large as 0.29 ± 0.05 and is a strong function of preparation procedures. These values for δ were also confirmed by fitting difference files obtained by subtracting the back-transformed data of EP AgO samples from that of CP AgO. The values of δ in Table IV correlate qualitatively with the broadening of the Bragg diffraction lines (Table II), and the Bragg peak broadening can therefore be attributed to vacant oxygen sites in the monoclinic AgO lattice.

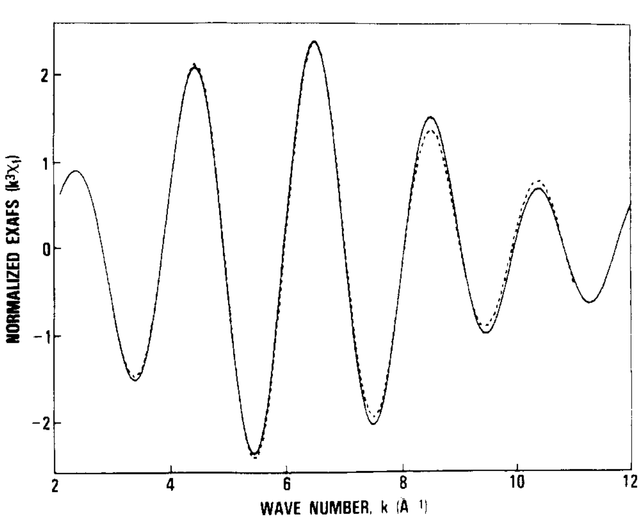

Figure 3. Inverse Fourier transform ($k^3\chi$ versus k) of the first peak in the Fourier transform of the experimental data (solid) for CP AgO compared with calculated spectra (dash) with use of parameters from a fit with two Ag–O shells.

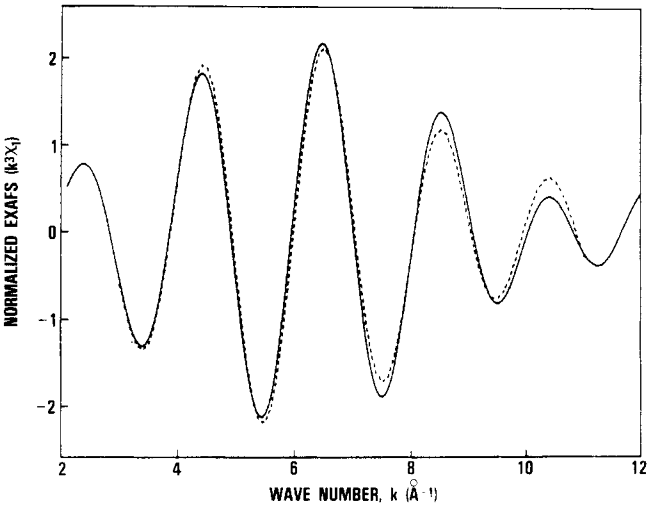

Figure 4. Inverse Fourier transform ($k^3\chi$ versus k) of the first peak in the Fourier transform of the experimental data (solid) for EP AgO (EP-5) compared with calculated spectra (dash) with use of parameters from a fit with two Ag–O shells.

The reduced amplitudes in Figures 1 and 2 and, hence, oxygen deficiency in EP AgO cannot be attributed to the presence of a mixture of metallic and oxidized silver. X-ray diffraction analysis showed that these samples consist mainly of an oxide phase and a small amount of metallic Ag (Table II). EXAFS analyses also indicate the presence of a small amount of metallic silver that is consistent with the XRD results. Futhermore, the presence of metallic silver should reduce the coordination number for both the Ag^+ and Ag^{3+} ions (N_1 and N_2) by the same percentage since they are present in the AgO lattice in equal amounts. However, this is not the case as can be seen from Table IV, where N_1 remained near 2 (N_1 for CP AgO) while N_2 varied from 2.8 to 3.5 oxygens, which is significantly less than 4 (N_2 for CP AgO).

A combined thermogravimetry–gas chromatography (TG–GC) compositional analysis on similar samples of EP AgO has revealed that Ag_2O can be present in large amounts (up to 37 mol %) in electrochemically prepared AgO material.[5] Similar analysis on the EP AgO samples investigated here has always indicated significantly larger amounts of Ag_2O than those determined by XRD. For example, according to TG–GC analysis, the EP-5 sample contains 31 mol % stoichiometric Ag_2O and 69 mol % stoichiometric AgO. These percentages for Ag_2O/AgO are much larger/smaller than those determined by XRD (Table II). If the Ag_2O/AgO percentages were accurate, then the number of Ag^+–O bonds (i.e., N_1 in Table IV), as determined by EXAFS, should be less than 2 since only the Ag^+ ions in AgO and not those in Ag_2O contribute to this type of bond. This would imply that for the EP-5 sample $N_1 = 1.38$. As can be seen from Table IV, however, this conclusion is not consistent with our results. In a forthcoming paper,[24] we show that erroneous conclusions result from TG–GC analysis when the assumption is made that only stoichiometric AgO is present in EP material. A new approach[24] based on a combined analysis by TG, GC, and XRD that takes into account the oxygen defect structure of AgO has been developed and has yielded conclusions in agreement with the EXAFS results presented here.

Our EXAFS results constitute conclusive evidence for the existence of a phase of silver oxide Ag_4O_3, which is found in electrochemically formed AgO. Samples EP-5 and EP-6 are mainly composed of this phase. The fact that the oxygen vacancies form preferentially at specific sites, is prima facie evidence that Ag_4O_3 is structurally distinct and must have a different heat of formation from a form of AgO in which the oxygen-vacant sites are randomly distributed between the Ag^+ and Ag^{3+} ions. The atomic structure of this phase is derived from that of AgO by creating one oxygen vacancy for each Ag^{3+} ion at sites that are adjacent to an Ag^{3+} ion but not to an Ag^+ ion. On the basis of the analysis of the discharge curves, Rollet[25,26] has conjectured that such a phase is produced in the anodic oxidation of metallic silver. To satisfy the condition for charge neutrality in this phase, Ag should be present in equal amounts of Ag^+ and Ag^{2+}, rather than Ag^+ and Ag^{3+}, which is the case in monoclinic AgO. We believe that, for $0.0 < \delta < 0.25$, silver oxide cathodes should be regarded as a mixture of AgO and Ag_4O_3. Thermogravimetric determination of decomposition kinetics has shown that Ag_4O_3 is thermally less stable than monoclinic AgO and its presence is a major source of thermal instability in EP silver oxide cathodes.[27]

The EXAFS results suggest that the electrochemical oxidation of Ag or Ag_2O to AgO may proceed via the formation of Ag_4O_3 as an intermediate phase. The formation of AgO evolves as a consequence of populating the oxygen-vacant sites in Ag_4O_3.

The existence of an Ag_4O_3 phase has scientific and technological impact that is not limited to battery technology. For example, in a study of the magnetic properties and crystalline structure of AgO by McMillan,[28] it was stated that "with respect to its property of semiconductivity, it should be emphasized that the value of the electrical conductivity is low and could be explained on the basis of an excess- or defect-oxygen lattice. There are, however, no experimental results to support this or any other assumption." To the best of our knowledge, the results presented here constitute the first direct experimental evidence for the existence of a defect-oxygen lattice that may explain the semiconductivity of AgO. Furthermore, the presence of Ag^{2+} or equivalently Ag^{3+} coordinated with only three rather than four oxygens is probably the origin of the paramagnetic centers that have been measured experimentally in EP AgO materials.[29]

In summary, we have determined that all EP AgO samples investigated consisted mainly of oxygen-deficient AgO (i.e., nonstoichiometric AgO). The oxygen-vacant sites are all located near the Ag^{3+} ions. The degree of oxygen deficiency, δ, can be as large as 0.29 ± 0.05 and depends on preparation conditions such as the metallic silver porosity and/or current density. A new phase of silver oxide, namely, Ag_4O_3, is electrochemically formed.

Acknowledgment. I thank Dr. C. R. Anderson for providing assistance during data collection at NSLS; Dr. S. Dallek, D. R. Glen, B. F. Larrick, and K. M. O'Neill for preparing samples no. 2–4; Dr. M. K. Norr for preparing samples no. 5–7 and the scanning electron microscopy micrographs; and Dr. R. N. Lee for his critical reading of the manuscript. This work was supported, in part, by the Independent Research Program of the Naval Surface Warfare Center. The X-ray absorption measurements were performed at NSLS, which is supported by the U.S. Department of Energy.

---

(24) Mansour, A. N.; Dallek, S. Submitted for publication in *J. Electrochem. Soc.*

(25) Rollet, A. P. *Compt. Rend.* **1928**, *186*, 748.

(26) Rollet, A. P. *Ann. Chim. (Paris)* **1930**, *13*, 137.

(27) Mansour, A. N.; et al. To be submitted for publication in *J. Phys. Chem.*

(28) McMillan, J. A. *J. Inorg. Nucl. Chem.* **1960**, *13*, 28.

(29) McMillan, J. A. *Chem. Rev.* **1962**, *62*, 65, and references cited therein.

ADDITIONS AND CORRECTIONS

1989, Volume 93

John M. C. Plane,* B. Rajasekhar, and L. Bartolotti: Theoretical and Experimental Determination of the Lithium and Sodium Superoxide Bond Dissociation Energies.

Page 3144. We regret that an error was made in calculating the lower limits to D_0(Li–O_2) in Table V. A corrected table appears to the right. The best experimental lower limit, including the diffusional correction used in the original paper, is thus D_0(Li–O_2) > 180 kJ mol^{-1}. This lower limit to the bond energy is now less than our ab initio value of 296 kJ mol^{-1}, and thus in better accord. The implication is that reaction 2 is still far from equilibrium under the experimental conditions employed. We therefore revise our recommended value of D_0(Li–O_2) from 306 kJ mol^{-1} to 296 kJ mol^{-1}.

TABLE V: Derivation of the Experimental Bond Dissociation Energies

[O_2], 10^{15} molecules cm^{-3}	k_{diff}/k'	K_{eq},[a] 10^{-15} cm^3 molecule^{-1}	D_0,[a] kJ mol^{-1}
	Li + O_2 + N_2		
1.85	0.45	6.16	201
3.70	0.28	4.31	200
5.55	0.12	2.67	194
7.40	0.09	1.49	188
	Na + O_2 + N_2		
5.0	0.10	23.7	213
9.9	0.04	11.6	206
19.8	0.02	11.5	206
24.7	0.01	11.5	206

[a] Lower limit; see text for discussion of diffusion corrections.